ABSTRACT

Title of Thesis: DESIGN AND FABRICATION OF A PHOTONIC MEMRISTOR USING A METAMATERIAL

Daniel Lay
Thomas Liu
Phillip Shulman
Humza Yahya

Directed By: Professor Min Ouyang
Department of Physics

A memristor is a nonlinear circuit element whose impedance depends on the history of current through the device. Photonic circuits are circuits that use photons rather than electrons to transfer signals. Memristors, then, exist in photonic circuits. With this in mind, we proposed, designed, and constructed the analogue of a memristor for use in a photonic circuit, in the infrared regime. The design focuses on an array of silver pillars, of varying pitch. The team's simulations indicate that changes in the pitch of the array modify the transmittance of infrared-regime light rays. After conducting these simulations, the team constructed a five-by-five array of polymer rods, with height 3.5 μm and pitch 5 μm, and coated in 100 nm of gold. We then immersed the array in various PNIPAm solutions. PNIPAm expands with increasing temperature around 32 ^{o}C, and so is thought to change the pitch of the array. This is the first use of a PNIPAm-based polymer to attempt to achieve a variable pitch, for use in a photonic memristor.

DESIGN AND FABRICATION OF A PHOTONIC MEMRISTOR USING A METAMATERIAL

by

Team META:
Daniel Lay
Thomas Liu
Phillip Shulman
Humza Yahya

Thesis submitted in partial fulfillment to the requirements of the Gemstone Honors Program, University of Maryland, 2019.

Advisory Committee:
Professor Min Ouyang, Mentor
Dr. Marina Leite
Dr. Anil Deane
Dr. Steven Anlage

Acknowledgments

We would like to recognize everyone who has supported and provided guidance to us throughout our project. First, we would like to thank Dr. Min Ouyang for his lasting support for our team research and individual endeavors. Next, we would like to thank the Gemstone staff, including Dr. Frank Coale, Dr. Kristan Skendall, Vickie Hill, and the rest of the support staff, who provided us with the opportunity to conduct research under the Gemstone Program. Additionally, we would like to thank our team librarian, Nevenka Zdravkovska, as well as our discussants Dr. Marina Leite, Dr. Anil Deane, and Dr. Steven Anlage for guidance in analysis of our data and ideas. Finally, we would like to thank our friends and families for supporting us.

Table of Contents

List of Figures

Chapter 1: Introduction

1.1 Overview

Research in many fields requires increasingly complex tools for all manner of computations and simulations, beyond even the capabilities of modern computers. This is due in some part to computers being based on electronic circuits. Photonic circuits use photons, rather than electrons, to transfer signals, and perform computations. These circuits can help fill in the gap in capabilities that exists. Moreover, memristors themselves can revolutionize electronic circuits: they are elements whose resistance depends on the history of the current through them, a property not utilized in current computers. There is an analogous component for photonic circuits, called a photonic memristor, that can similarly revolutionize photonic circuits. For these reasons, the team tasked itself with fabricating a photonic memristor, to function in the infrared (and later, the visible) regime.

1.2 Purpose

Photonic circuits are primarily useful for data transfer and processing. It is impossible to exceed the speed of light, which makes light the quickest way to deliver

information. Faster transfer of information will revolutionize how data servers are designed, and provide significant increases in the power of parallel computing, by removing limitations on the size of computer clusters. Recent photonic circuits can carry information one hundred times faster than conventional copper-based circuits. In addition to greater information transfer speeds, photonic circuits provide increased bandwidth, allowing for a greater amount of information transferred at once.[1] Besides simple data transfer, to maximize efficiency of a light-based data transfer system, photon-based computing systems should be used in tandem with the transfer system, so as to avoid the necessity of converting the information to and from electronic signals.[2] This means that the development of light-based computing systems, in any possible form, is a necessity for computation and data transfer.

The name memristor comes from the phrase memory resistor, due to how it interacts with current flow. Electronic memristors remember and alter their resistance based on the history of the current that has passed through them.[3] Similarly, photonic memristors remember and alter their impedance based on the power of light transmitted through them. One potential application for a photonic memristor is a novel type of random access memory (RAM), that uses substantially less power than conventional RAM, called non-volatile RAM (NVRAM). Preliminary simulations suggesting up to 27% power savings over conventional RAM.[4] One other application that will be discussed later is an analog circuit. From these applications, it is clear that memristors are immediately quite useful, even in everyday computing. Besides this, the photonic memristor proposed here provides further functionality to photonic circuits, rather than just electronic circuits.

Memristors have been constructed for microwave frequencies, e.g. by Wu et. al. in 2014. This work used a metamaterial as the basis for the memristor.[5] For visible frequencies, memristors have also been constructed, e.g. by Hoessbacher et. al. in 2014.[6] Not only was this structure not based on a metamaterial, no memristor for the visible range has been constructed using a metamaterial. From this fact, and the above applications, a natural next step is the creation of a metamaterial that acts as a memristor that functions in a photonic circuit operating at visible light frequencies. For reasons that will be elaborated on later, the team decided to focus on the infrared regime first, rather than the visible regime. This leads to the research question: how can a metamaterial that acts as a memristor for photonic circuits at infrared frequencies be created? To answer this, an additional question must be answered: what constituent materials, and in which arrangements, can be used to create a metamaterial that acts the desired memristor?

Chapter 2: Literature Review

Understanding our approach to the creation of a photonic memristor requires a background in photonic circuits, memristors and metamaterials. In order to understand photonic circuits, relevant electromagnetic theory will be described, and a comparison between photonic and electrical circuits will be established. From there, an understanding of memristors will be facilitated, so the reader will understand how memristors impact the functionality of photonic circuits. Finally, we will explore the way in which metamaterials can be used in the creation of a photonic memristor, by understanding some general properties of metamaterials and their applications.

2.1 Electricity and Magnetism Review

Photonic circuits operate with light of specific frequencies, depending on the design of the circuit. Microwaves, infrared waves, and visible waves are all frequencies of electromagnetic waves, so one can consider them as a single case, with regards to how the photonic circuit functions. Many applications carry between the regimes as well. Differences between the regimes will be discussed later. To understand photonic circuits, and later metamaterials, a brief theory of electromagnetism is required.

Light waves of all frequencies are composed of varying electric and magnetic fields that oscillate sinusoidally and travel at the speed of light. In Maxwells equations, which express all electromagnetic phenomena, there are the physical values μ, the magnetic permeability, and ϵ, the electric permittivity. The magnetic permeability describes to what degree the media supports a magnetic field, with greater values supporting stronger fields. The electric permittivity expresses how much energy is needed to polarize a medium, which is proportional to the degree of resistance the material expresses to changes in electric fields. Larger permittivity denotes greater resistance of the media. Empty space has a permittivity and permeability, written as ϵ_0 and μ_0. Other media, such as water or copper, have different functional permittivities and permeabilities, and thus use different values to describe optical currents movement through them.

The functional permittivities and permeabilities are also used to describe how wave propagation changes when light moves between media: Snells law states that waves leave a media at an angle dependent on both the angle of incidence and the medias refractive index. Moreover, the refractive index characterizes the speed of light through the substance. The refractive index is dependent on the real parts of the medias permittivity and permeability. By controlling these values, and hence the refractive index, light propagation within a medium, such as a photonic circuit, can be finely engineered.

Most non-metallic materials have a permeability on the order of 10^{-6} H/m, while metals, especially specifically engineered ones, can reach permittivities a million times larger. Electric permittivity is universally larger than ϵ_0, but in metals

is difficult to separate from conduction, and therefore measure. This leaves a wide range of values that are not found in nature, and all materials that have these unnatural permittivities and permeabilities are classified as metamaterials. The real parts of the permittivity and permeability of certain metamaterials are negative.[7] However, the values for μ and ϵ can vary beyond both being negative, including having opposite signs, both being zero, and both being equal and positive.[8] Each of these has different applications, and is a field in and of itself. The team's focus is on a varying, positive permittivity, and a constant positive permeability, as in the recent experiment by Malerba et. al., in which the permittivity of their metamaterial varies with a change in geometric properties of the structure.[9]

2.2 Photonic Circuits

Photonic circuits are, in some ways, similar to conventional electrical circuits. The transmitted power is akin to the current, and the structures that the light interacts with along the path of the beam act as circuit components. Such structures include analogues to resistors and capacitors in electronic circuits. The main parameter determining the properties of such a structure, rather than the conductivity and geometry, is the electric permittivity. This number is complex: the real component is the equivalent of electrical resistance, and has a linear relationship with energy loss. The imaginary component corresponds to the delay between the application of an electromagnetic force and the reaction of the material. This distinction arises from the non-instantaneous nature of medias response to changing

electric fields. If the imaginary part is positive, the particle will act as a capacitor in addition to its impedance loss. If the imaginary part is negative, then it will act as an inductor, again with the impedance loss. The permittivity describes other components as well, such as connective wires. These wires consist of a very permissive media, called epsilon-near-zero (ENZ) material, surrounded by very exclusive media, called epsilon-high-value (EHV) material. The difference between the permittivities of the ENZ and EHV materials causes total internal reflection, guiding the light beams along a set path, according to the properties of electromagnetism described above. Hence, these structures are called waveguides. These components can be combined to form information circuits, which apply changes to input waves that can be interpreted as operations on a given function.[1]

The basic theory behind photonic circuits is relatively well-established, compared to that of memristors. Moreover, the creation and use of simple photonic circuits for information transmission, in the form of fiber optic cables, is well established, and has been researched extensively for decades, from at least as early as 1986.[10] Fiber optic cables are classified as photonic circuits as they both use waveguides to control the light. Fiber optic cables are used worldwide, on both small and large scales, although they have not replaced traditional means like radio or satellite transmissions, which are more specific for long scale information transmission. Currently, however, there are no commercially available computers that utilize photonic circuits, due in large part to the difficulty associated in designing components. For instance, as recently as 2016, NOT and NOR logic gates were still being researched and analyzed as new items.[11,12] These basic components are used

extensively in logical systems, especially computers, so their lack of availability in photonic circuits helps explain the lack of photonic circuit-based computers.

With that said, some logic gates and individual components, have been successfully constructed many times.[1,12,11] While the construction of the analogues to resistors, capacitors, and inductors is well established, the same cannot be said for memristors. Preliminary results in the construction of memristors for photonic circuits have shown moderate success.[6] To understand recent developments in the field of memristors, memristors themselves must be understood. In order to facilitate this, the theory involving memristors in electrical circuits will be discussed. Then, as in the discussion of photonic circuits, photonic memristors will be considered in comparison to electrical memristors.

2.3 Memristors

The existence of memristors in electrical circuits is founded from a logical gap in the circuit theory. In this formulation, circuit elements are defined by their relationships between current, voltage, charge and flux-linkage. Three of these relationships describe the fundamental passive circuit elements: resistors relate current and voltage, capacitors relate charge and voltage, and inductors relate the flux-linkage and the current. The next two are the definitions of charge and flux-linkage: charge is defined as the history of the current that has passed through it, and flux-linkage is defined as the history of the voltage that has gone through it. The relationship between charge and flux-linkage is represented by the memristor. The resulting

functionality is a component that acts as a resistor, whose resistance depends on the charge that has gone through it.[3,13]

To determine if an object is a memristor, a hysteretic loop can be created. Building a hysteretic loop involves exposing a media to a powerful, slowly oscillating voltage source and measuring the current. When the voltage returns to its original value, a loop is formed, the shape of which characterizes the circuit element. In a normal resistor, for instance, the loop is actually a curve, as there is one value of resistance for every tested power (and, for typical resistors, the curve is actually linear). Figure 2.1 (a) is one such example. On the other hand, for memristors, the curves for the power up step are different than that of the power down step, resulting in a pinched hysteretic loop,[5] as shown in Figure 2.1 (b). A non-volatile nature results from having a different resistance in the power up and power down steps, which leads to the applications mentioned in the introduction: NVRAM and analog circuits.

Measuring an optical components loop would involve exposing the media to light and tracking transmittance, but the overall thought process is identical. Photonic memristors change their electric permittivity (analogous to the change of resistance in electrical circuits) based on the electric and magnetic fields that they have been exposed to in the past,[1] as mentioned when describing photonic circuits. When this happens, the hysteretic loop mentioned before is formed. This is what determines if the object is a memristor. Due to the non-volatile nature, some applications, including NVRAM and analog circuits, are the same.

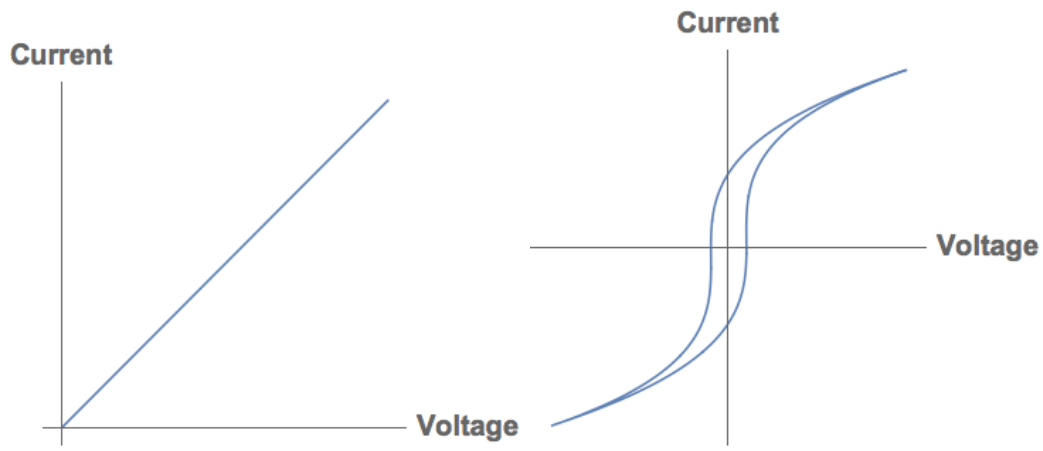

(a) Typical (i.e. non-memristive) voltage vs. current profile.

(b) Sample memristive voltage vs. current profile.

Figure 2.1: Contrast between the $V-I$ profile for a non-memristive and a memristive system. The hysteretic loop was parametrized using Equation (1) of Lapshin's review,[14] with $m = n = 3$.

2.3.1 Memristor Applications

One application for memristors, as mentioned above, is NVRAM.[15] NVRAM is a specification of non-volatile memory, which is essential for providing storage for future computing.[16] More specifically, it is defined as RAM that retains its information when power is turned off, and updates only individual components in the memory when performing a step in a computation. This is in contrast to many widely used RAM technologies that must update the entire device when used.[17]

As memristors relate the flux-linkage to the charge, they have a non-volatile nature, which means that the entire component does not have to be updated. Because of this property, memristors can be used to construct NVRAM: memristors can be in a state that does not update entirely in any given computing step, which is a defining property of NVRAM.[16] Incidentally, the data will also be maintained

when power is lost, since the non-volatility is not dependent on any voltage source.[17] Since the entire device does not have to update every time a calculation is required, less energy is required than conventional RAM.[4] While the above description is only strictly accurate for electrical circuits, the properties still apply to photonic circuits. Specifically, memristors serve the same function in both, albeit defined differently, meaning that photonic memristors can be used to create a photonic analogue of NVRAM.

Aside from NVRAM, memristors have been theorized to be capable of replacing transistors, in the form of analog circuits. Analog circuits take on a continuous value instead of a binary value. So, a single analog circuit serves the role of many transistors. Due to a varying resistance, memristors (both electronic and photonic) can serve as analog circuits. As photonic circuits require all components to be printed with a waveguide, memristors can greatly simplify large components into a single element.[1] When miniaturized, photonic memristors can lead to large advances in fiber-optic computing. This simplification will further add to the miniaturization of modern circuits and can greatly increase processing power and efficiency.[15] Other possible applications of memristors include aspects of machine analysis, neural network development, sensor development, and edge detection/image processing.[18]

2.3.2 Photonic Memristors

While the above applications certainly hold for electrical circuits, the team is concerned with the application of memristors to photonic circuits. The physics

involved in explaining these applications is quite different, but photonic circuits and electrical circuits can be designed for the same purpose and equivalent, so it is no surprise that these properties can be created with photonic circuits.[15]

While there have been multiple memristors created for electrical circuits, such as the one created by Shin, Kim, and Kang in their construction of an analog circuit using electrical memristors,[19] there have been relatively few created for photonic circuits. One was recently demonstrated for photonic circuits at visible frequencies by Hoessbacher et al., in which a memristor was fabricated to operate as an optical switch. The device was fabricated using photolithography, a method to be described in the metamaterial section, but was not made out of a metamaterial. Hysteresis was measured, indicating that the construct is a memristor, and can be used for an optical switch.[6]

For microwave frequencies, as mentioned above, Wu et. al. have constructed a photonic memristor, meaning that a hysteretic loop was observed. Here, however, the memristor was constructed using unit cells connected together in the shape of a cube, of side length 2 mm, and these were then attached to each other in an array of 5 mm by 5 mm squares, with space in between each of the smaller cubes.[5] This is classical metamaterial behavior, by definition: the memristive property would not occur without the cells being connected together in this manner. This shows that metamaterials can be used to construct memristors for photonic circuits.

2.4 Metamaterials

Metamaterials are a promising tool for creating memristors. They are a class of objects specifically engineered to have small-scale properties that result in a desired macroscopic effect. They are constructed using unit cells that are much smaller than the wavelength of the waves with which they are designed to interact. These cells are arranged in a geometric pattern, and the combination of the pattern and the constituent materials gives the metamaterial the desired properties.[20] This is the motivation for our research question involving materials and geometric structures, as these must be determined to design any metamaterial. As the team is concerned with metamaterials as they relate to photonic circuits and memristors, the waves that are discussed are light waves, and so the metamaterials obey the laws of electromagnetism as described above.

By varying the geometry and composite materials at the micrometer scale, a specific macroscopic effect can be achieved. Due to the large number of variations of these properties, metamaterials have an incredible number of theoretical applications. Furthermore, many interactions with light depend on the frequency of the light involved, which further increases the variety of possible applications. An application of metamaterials that is especially of interest to the authors is the creation of a memristor for use in a photonic circuit, for light at infrared frequencies.[5] Below, both microwave- and visible-frequency metamaterials are discussed: microwave-frequency to provide an overview of the topic, and visible-frequency to highlight some difficulties with fabricating visible-frequency metamaterials.

2.4.1 Microwave Metamaterials

Sir Pendry set the stage for microwave metamaterials by creating a microstructure of split ring conductors made of copper that were much smaller than 0.1 cm, the smallest wavelength at which light is still in the microwave band.[20] This allowed the metamaterial to concentrate the electromagnetic energy from the microwaves, and showed that microstructures can result in a negative magnetic permeability. By 2000, a metamaterial that had negative permeability and permittivity in the microwave frequency was created using split ring resonators, and split ring resonators are still a basis for many metamaterials operating in microwave frequencies.[21] This work helped lay the foundations for the field of microwave metamaterials.

The first tunable microwave metamaterial was created in 2002, using a mesh of thin metallic wires. The research group realized they could modify the composition of the metamaterial to change the frequency of microwave emission that is sent out, thus tuning it to react to specific frequencies. The group also theorized that advances made in microwave metamaterials could be used to create metamaterials with specific properties that operate in other wavelengths.[22] By 2008, researchers were able to control which frequencies metamaterials emitted and absorbed.[23] The ability to tune has been used in many metamaterials that have been created since, notably including the microwave-frequency metamaterial developed by Wu et al. in 2014.[5]

Modifying the composition of the metamaterial is not the only method to tune the metamaterial to specific frequencies. A 2003 patent outlined a method

using tuned filter layers, as a relatively simple, loss-free dielectric media for large parts of the microwave spectrum. The material is comprised of periodic layers of specific dielectric components. In this way, a barrier can be engineered to exclude all microwaves except those near the desired wavelength. This barrier can then be used to improve signal clarity of specific wavelength transmissions. Alternatively, a barrier could be produced to isolate an experiment from a microwave frequency that would produce a false signal, thereby improving the accuracy and precision of the instrument.[24]

Aside from memristors, there are many other applications of microwave metamaterials. Techniques using active gain in the form of a waveguide, which confines the microwaves, increase the signal and reduce the effects of loss. As photonic circuits use waveguides to guide the signal, the paper by Ye et al. demonstrates that metamaterials can be created with a waveguide component, which is a key component of memristors that will be used for photonic circuits.[25] Additionally, active gain microwave metamaterials are a useful stepping stone in applying methods learned at the microwave wavelength to shorter wavelengths like the visible spectrum. Recently the miniaturization powers of metamaterials were demonstrated by creation of a miniaturized metamaterial antenna measuring 16 mm by 21 mm by 1.6 mm.[26] Although this is far from small enough to be used in the visible (or infrared) frequencies, to some extent, it shows the power of applying techniques created for microwave frequencies to higher frequencies (e.g. infrared or visible).

Many of the described metamaterials are created in similar ways. First, a unit cell of a certain pattern is created, which dictates the properties of the metamaterial.

The unit cell is then repeatedly printed on a substrate, for instance thin copper layers a few millimeters thick. In some cases, these layers are stacked to further refine their properties.[27] As microwave metamaterials often use wires or unit cells a few millimeters thick, they can be designed and 3D printed in the desired pattern, even when made of metal.[28] This approach readily extends to the infrared regime. However, it does not extend to the visible regime.

2.4.2 Visible Metamaterials

This section of the literature review serves to demonstrate some of the technical considerations associated with fabricating any object for use in the visible regime. While the team initially considered constructing a photonic circuit in the visible regime, the challenges below forced the team to consider construction in the infrared regime instead, in which many techniques used for microwave frequencies are applicable. The reader should take care to recall that our design and implementation are for metamaterials in the infrared regime.

While some design techniques from microwave frequencies can be used with visible frequencies, manufacturing techniques cannot. Visible light has a wavelength between 400 and 700 nanometers. As mentioned previously, the unit cells must be smaller than, or approximately the same as, the wavelength that is considered, so for the visible spectrum, unit cells that are on the nanometer scale on each side are ideal for many constructs. For instance, simulations from a design involving lengths less than 30 nm on each side result in an absorption of over ninety percent throughout

the visible spectrum, which demonstrates that this length scale is successful.[29] As such, for fabrication on a scale of this size, many specialized techniques are required.

There are two different classes of metamaterial fabrication: top-down and bottom-up. Top-down fabrication includes all techniques that involve taking larger materials and removing matter to achieve the desired structure. Whittling away at wood to get the desired shape is an apt analogy for the process. Bottom-up fabrication includes all techniques that use building blocks, in the form of other nanostructures or atoms, to assemble the desired structure in three dimensions.[30] There are merits and drawbacks to both classifications. Top-down approaches are very well established and understood, and can make very detailed structures. Bottom-up approaches are capable of making structures that are dense, uniform, and three dimensional. Unfortunately, many top-down approaches are so costly that most metamaterials produced are limited to two dimensions. And, many bottom-up techniques are recently developed, so structures that are created lack some desired traits.[31]

A common example of top-down construction is electron beam lithography. This involves shooting electrons at a resist film, which is a film that reacts when exposed to light and other compounds, to store a pattern. Using a lift off technique, it is possible to remove the completed structure from the resist, to allow the structure to stand alone.[32] One such example is described in a June 2016 paper by Dong et al. Electron beam lithography was used to pattern the resist film, at which point titanium and aluminum layers, each less than 65 nanometers thick, were deposited. The metamaterial was then removed using a lift off technique, as mentioned above. This method created a metamaterial with strong absorbance across the visible spec-

trum. However, the result is very thin, and requires an additional grating structure in order to reach the high absorptance levels mentioned in the paper.[33]

Many common bottom-up techniques also involve using a top-down approach in order to create the desired structure. Molecular self assembly involves creating a two dimensional layer of molecules that will assemble itself into the desired object when the correct initial conditions (e.g. temperature and pressure) are applied. The layer of molecules is initially created by a top-down process, such as electron beam lithography. In order for the molecules to assemble on their own, the top-down process must be applied to a layer made of a specific combination of molecules, such as aluminum oxide (Al_2O_3), in order to guarantee that the process will be spontaneous. In this way, intermolecular forces between the systems cause them to spontaneously assemble into the desired item.[30] This was achieved by Robert Nidetz in 2012, when his experiment reached equilibrium self-assembly in twenty minutes, by immersing the templates into a gold nanoparticle solution.[34]

A similar method is the use of Atomic Layer Deposition in combination with deep reactive ion etching.[35] Atomic Layer Deposition consists of depositing one layer of atoms at a time. Between each layer deposited, a substrate is used to remove excess atoms of the same type as the layer just deposited. This process yields a very precise structure, but the process can be costly, and the deposition process is very slow.[30] The experiment was focused around fabricating titanium oxide (TiO_2) and Al_2O_3 in a nanolayer structure. These materials were layered upon a silicon template, and subsequently etched down to the desired height. The scientists successfully created the nanostructures and concluded that this method

has potential for being able to modify the structure to achieve the desired properties at the visible scale.[35]

From the above literature review, it is clear that photonic circuits, memristors, and metamaterials are each a rich field. Before transitioning to the team's usage of each of these, however, one more topic must be introduced: thermally responsive polymers.

2.5 Thermally Responsive Polymers

Thermally responsive polymers are polymers that undergo a drastic change in properties in response to a change in temperature. An important (and perhaps the primary) class of applications of thermal polymers is to the biomedical field. These polymers can be used in drug delivery, as carriers of drugs to locations in the body. Upon arrival and stimulus the drug is released in the desired concentration. For instance, a temperature increase may cause a volume change and let the drug diffuse into the body. Applications to gene delivery and tissue engineering use similar techniques.[36]

While many types of change are possible, one of particular interest to the team is a change in volume of a polymer. The origins of this volume change are not discussed here, although they have been studied extensively.[37] Such a volume change translates to a change in solubility. Polymers that become less soluble above a certain temperature are said to have a lower critical solution temperature (LCST), while those that become more soluble above a certain temperature are said to have

an upper critical solution temperature (UCST). These polymers are then labelled as LCST or UCST polymers, respectively. Examples of LCST polymers are those based on Poly(N-isopropylacrylamide) (PNIPAM) or Methyl Vinyl Ether-Styrene (MVE) monomers.

Generically, the solubility of polymers depends on factors including the temperature, the molecular weight of the polymer, and the concentration of the solution. Some polymers undergo a phase transition at a temperature near LCST, regardless of the concentration or the molecular weight.[36] For this reason, the two temperatures are often used interchangeably. NIPAM-based polymers specifically have been observed to have an LCST, above which the polymer exhibits a drastic change in the intensity of scattered light, among other properties.[38,39] More precisely, NIPAM-based polymers used in a study by Zhou et. al. were observed to have an LCST of approximately 32 °C, above which the average scattered intensity is roughly 5 times that of the intensity below LCST. Additionally, the electric permittivity of various polymers depends on both the frequency of the light and the temperature of the solution.[37] Among the polymers used, it was true that polymers at temperatures above LCST have a lower permittivity than those below LCST. Moreover, the permittivity decreased with increasing frequency, asymptoting to a value of $\varepsilon' \sim \mathcal{O}(10^2)$. More generally, many NIPAM-based polymers exhibit an LCST between 30 and 34 °C in an aqueous solution, regardless of differences in particular properties, such as a different end chain on the polymer.[36] Due to the approachable LCST, and the volume change at this temperature, of NIPAM-based polymers, the team chose to use solutions of this kind to attempt to achieve a memristive effect.

Chapter 3: Methods

Following the literature review above, and keeping in mind the research questions, the team decided to create arrays of nanorods, as in the work by Malerba et. al. As shown in that publication, the arrays had a certain frequency where the radiation properties, especially reflectivity, suddenly decreased. This decrease is at a wavelength that depends on the pitch of the array.[9] Our array would be set up with a dynamic pitch, that changes with the temperature. As the array is exposed to light, it should heat up as it absorbs photons. This absorbed heat would therefore change the pitch. While in Malerba et. al., changing the pitch required a whole different array each time,[9] our proposed array would change its behavior over time as it is exposed to light. When submerged in a PNIPAM solution, which expands rapidly in between 30 and 34 °C, the array would be pushed apart by the expanding liquid, provided it was sufficiently viscous. This is the effect shown in Figure 3.1, although there it is dramatized for effect. The movement of the rods would increase the negative space between each rod, which would change the resonant frequency of the array. It was hypothesized that, for a frequency close to the resonance of such an array, one would see a significant change in the transmission as the rods are forced apart.

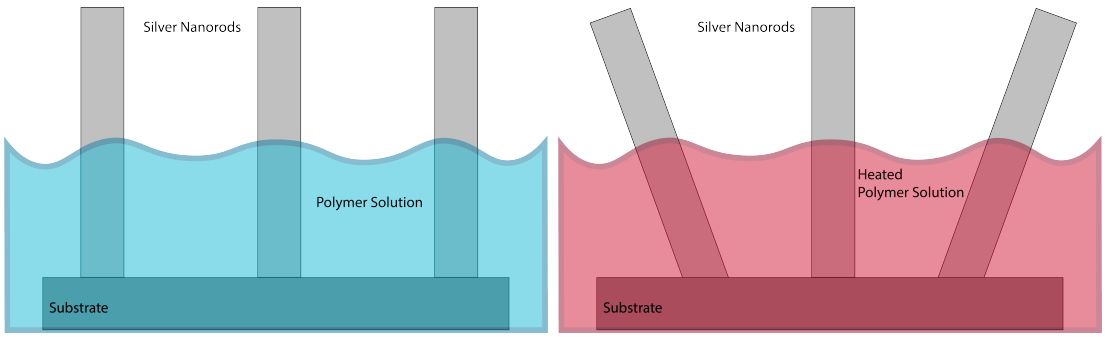

(a) Above is the proposed geometry with the polymer below LCST.

(b) Above is the proposed geometry with the polymer above LCST.

Figure 3.1: The proposed effect that should occur upon heating the polymer. Dramatized for effect.

Prior to testing this effect, the team confirmed Malerba et. al.'s results,[9] using numerical simulation techniques detailed below. The team did not simulate the tops of the pillars spreading, due to significant technical difficulties in constructing such a situation in the software used. After these simulations, the team attempted to construct an array with an effectively variable pitch, using a thermoresponsive polymer solution. The extent of the experimental progress is detailed below, after a discussion on the simulations.

Briefly, a second idea was considered. The team considered constructing an array of silver nanorods, encasing these in a mica layer with an indium substrate, and placing a gold layer on top of the entire structure. While preliminary simulations were conducted for this idea, immediate fabrication concerns (mainly dealing with mica) forced the team to pursue the thermoresponsive polymer idea.

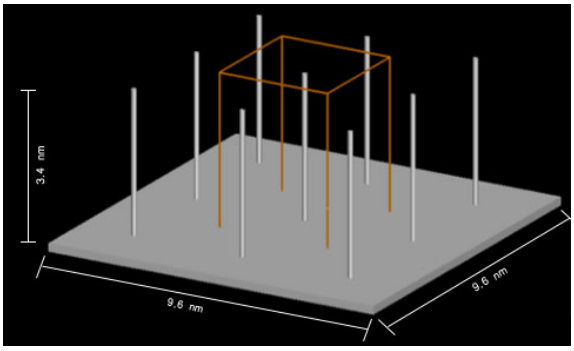

Figure 3.2: The initial simulation setup of the silver nanorod array. Note that the dimensions are in nanometers.

3.1 Simulation

Potential geometries were simulated using Lumerical FDTD Solutions.[40] Initially, the simulated geometry was a scaled down, slightly different, version of the silver nanorods constructed by Malerba et. al.[9] One difference between the nanorods is that Malerba et. al. simulated rods with a hollow cavity, whereas the team simulated solid rods.[9] This was done because the construction of solid rods is simpler than the construction of hollow rods, especially when it comes to coating the array, which is discussed later. Additionally, the arrays were simulated for use in the visible regime, with wavelengths in the hundreds of nanometers. To achieve this effect, the dimensions of the array used by Malerba et. al.[9] were shrunk to this regime. The geometry of this simulation is shown in Figure 3.2, with an orange box highlighting an individual unit cell. A better understanding of the physical construction methods available to the team, and a desire for the simulations to match the experimental measurements, convinced us to change the dimensions of the simulated array to match those of Malerba et. al., on the micron length scale.[9]

The geometrys radiation properties were simulated using the Finite Difference Time Domain (FDTD) method. Initially the array was a finite, five rod by five rod arrangement, similar to that shown in Figure 3.2. However, the simulation was slow, inefficient, and unreliable. The relatively small size of the array relative to the length scales of the problem caused boundary conditions to dominate the simulation results. Using a single nanorod with Bloch boundary conditions not only severely reduced required computation time, but also gave reliable results. Bloch boundary conditions take the unit cell as an infinite array of unit cells, and therefore ignore boundary conditions entirely. While this is not physical, a large number of unit cells in a periodic pattern approximates an infinite array. Possible differences are small, and can be made smaller with larger arrays. These simulations tested various pitches around 5 μm and heights around 3.4 μm. These numbers are arbitrary, so long as they are close by this scale. 3.4 μm was chosen because this was a value that appeared to have a noticeable effect when analyzed by Malerba et. al.[9] The results are discussed in Section 5, with the individual simulation results. An example of the simulation region is shown in Figure 3.3. Note that the dimensions are in nanometers; this corresponds to simulations conducted prior to considering fabrication methods. Note also that the light is incident at an angle, shown by the purple arrow.

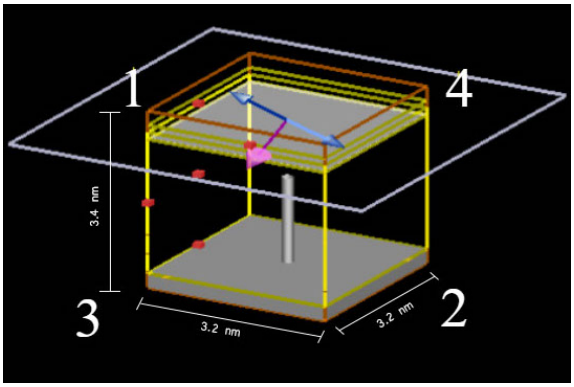

Figure 3.3: A sample simulation region using Bloch boundary conditions. The numbers 1-4 indicate the numbering on the monitors surrounding the region.

3.2 Fabrication

After preliminary simulations, the team began fabricating the array. This methodology is discussed below.

3.2.1 Array Construction

Due to technical considerations, the arrays constructed by the team were slightly different than both those constructed by Malerba et. al.,[9] and those simulated above. The two primary differences are the scale of the arrays, and the material used to build the array. The arrays were chosen to function in the infrared region (i.e. have reflectance minima corresponding to wavelengths in the infrared band), similar to those by Malerba et. al..[9] The array was 3D printed using a polymer, and was coated in gold, rather than being made of solid silver.

Pillar arrays can be constructed without much difficulty to function in the IR region, as Malerba et. al. demonstrated,[9] and in the visible region, using methods described in the literature review. As discussed previously, when constructing a

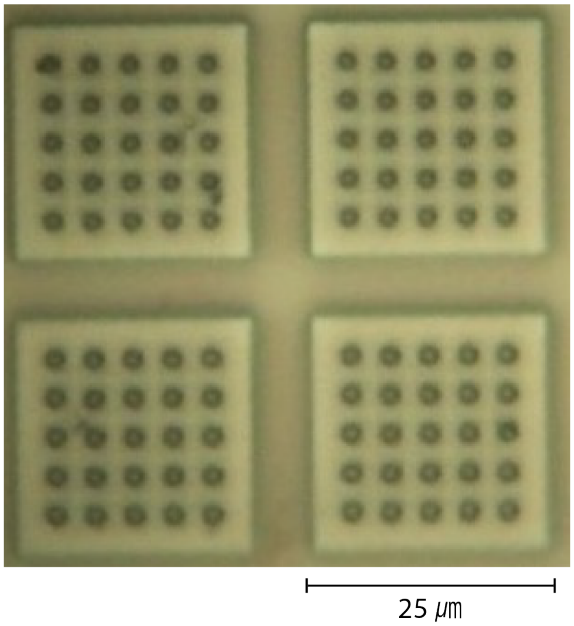

Figure 3.4: One of the slides printed out, viewed under a microscope. The magnification is 100x.

metamaterial, the unit cell must be smaller than the wavelength of light where the effect must occur. For an array to function in the infrared region, unit cells can be constructed with dimensions approaching 10 μm and still provide the desired behavior. For the arrays considered here, the unit cell is one single pillar, plus some region of the substrate it is constructed on, as shown in orange in Figure 3.2. Each unit cell was chosen to be a solid cylinder 1 μm in diameter, printed on a square 5 μm $\times$ 5 μm substrate. The actual structure built was a 5×5 array of these unit cells. Due to the size of the array, each was able to be 3D printed using the Nanoscribe equipment available at the University of Maryland.[41] Two batches of arrays were printed. The first consisted of 4 arrays to a slide, and 3 slides of arrays; the second was 5 slides of arrays, with the same number per slide. An image of one of the slides can be seen in Figure 3.4.

As mentioned briefly above, the Nanoscribe does not print metal, but a type of polymer. This is in contrast with the simulations conducted, in which the rods were treated as solid silver. So, the team added a thin layer of metal coating to the arrays after they were printed, using a sputter coater available through our mentor's lab. Gold was chosen rather than silver for a few reasons. The first is availability: the sputter coater available only is able to use gold. So, without finding substitute equipment, that is all that is available. The second is longevity: silver tarnishes, while gold does not. The experiment took enough time that silver could tarnish, and this is not an effect the team could prepare for, especially when simulating the expected results. Given an unlimited supply of arrays, this could still have been an issue, as one particular array might not remain untarnished even between coating and measuring. As there was no way for the team to quantify the tarnishing effect, a silver coating was ignored at the time. Finally, it was assumed that gold and silver coatings would yield a similar effect. While this should have led to further simulations, the team continued on with this line of thought: even in the event that a gold coating does not demonstrate the desired behavior, future arrays could be coated in silver (despite the possible issues mentioned above), and the rest of the methodology simply followed through.

To coat the arrays, the sputter coater was first calibrated to deposit roughly 4 nm of gold for every 20 seconds of run time. This number is not exact: in general, the deposition rate depends on a number of factors, including the position of the array within the coater, the temperature, and the pressure. Two arrays were then coated with a gold layer of thickness approximately 100 nm and 150 nm. The thickness is

liable to vary across the array, due to the randomness of the coating process. For this reason, a thickness too far below the chosen value may leave some parts of the array uncoated entirely. This sets a lower bound on the allowed thickness. The thickness chosen is sufficient to avoid these effects, meaning that light interacts with the array as if it were solid gold. On the other hand, there is an upper bound as well. The sputter coater has a maximum run time of 5 minutes. Additional gold coating should be added before the existing coating solidifies, else it may not stick to the array as desired. In this case, the thickness of the coating is unchanged, despite the coater running for a longer time period. Despite this, two runs can be attempted if they are done in immediate succession, as was done here. It is believed that the coating layer is truly the desired thickness, however no calibration check was done.

At this stage in the construction, the arrays are still visible under a microscope, even at a magnification of 4x. Due to the gold coating, a desk lamp is required to actually view the arrays, whereas previously, a light source below the array was sufficient. An array with gold coating is shown in Figure 3.5. Qualitatively, the reflection of the array in the desk lamp assured the team that some level of coating was achieved.

3.2.2 Polymer Addition

A few grams of a PNIPAM-based polymer was purchased from Sigma Aldrich.[42] The polymer was dissolved in heavy water (D_2O) in different percent-by-weight concentrations. It was observed that concentrations at or above approximately 40%

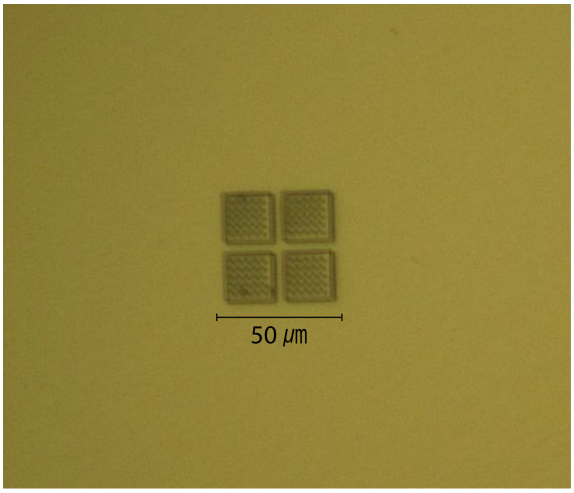

Figure 3.5: A coated array viewed under a microscope, with magnification of 10x. Note the lack of detail compared to Figure 3.4.

were difficult to manipulate and did not flow easily, and so the concentrations used later were far below this. Upon heating the solutions to their LCST, the solutions appeared noticeably different from those below LCST. Below LCST, the polymer solution was clear, as if no polymer were present at all. When heated past LCST, the solution expands and turns a milky white. This can be seen in Figure 3.6. Qualitatively, a slight volume change was noticed. However, this effect was not established quantitatively by the team. Rather, the cited literature was trusted as sufficient proof of a volume change.[39]

The coated arrays were then covered in the solutions created. Initially, low concentrations (roughly 5%) were applied, simply because more low-concentration solution was prepared at the time. To actually apply the polymer, a micropipette dripped up to 3 μL of the solution on the slide, near the array. The solution was then dragged across the array using the tip of the micropipette. This process was carried out under a desk-lit microscope, to ensure the solution actually enveloped

Figure 3.6: One concentration of the polymer solution, before and after being heated past its LCST. Note the white, milky appearance of the solution at temperatures above LCST, indicating the phase transition.

the array. It was believed desirable to not cover the array entirely with the solution, for fear of obscuring the desired effect. Simply put, if the polymer solution does block a good deal of the light, the bit of array above the solution may still provide a memristive effect. To ensure the solution was not entirely covered, the reflection of the desk lamp was used: if the solution was applied correctly, the reflection of the light off of the top of the array should still be visible. An additional confirmation is that the exact height of the array required to focus on the solution and to focus on the top of the array should be different. Both of these were observed when putting the solution onto the array, although the process is nontrivial. An image of the solution enveloping the array is shown in Figure 3.7. As an additional note, the amount of solution applied appeared to evaporate in less than 20 minutes; this was not considered a critical issue.

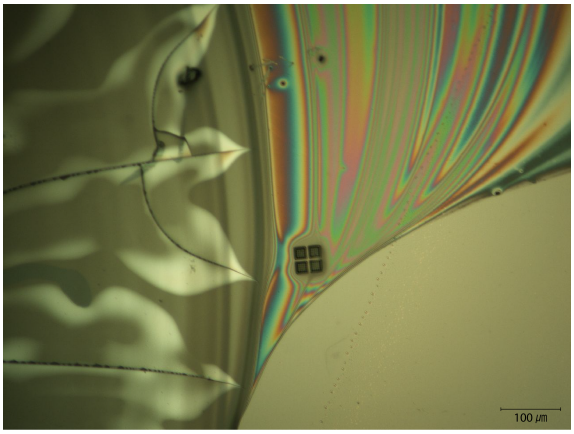

Figure 3.7: The solution partially enveloping the array. Due to the method of image capture, the reflection of light off of the top of the array is not visible. Some scratch marks appear, due to dragging the solution across the slide and over the array.

3.2.3 Measurement

The next steps in the process focus on measuring the effect quantitatively. Due to logistical issues, the team was unable to follow through on these measurements. However, the next steps in the process are described here. While in actual operation the array would be heated by absorbing incident light, the team will heat the array with a resistive heating element (a resistor that heats when a voltage is applied). This lets us control the temperature of the array more accurately, since measuring the temperature of such a small volume of liquid without disturbing it too much is not possible. The heating element was to be calibrated using a thermal couple, in order to determine which voltage should be applied to reach PNIPAm's LCST. In addition, the couple was to remain attached to the heating element, in order to monitor the temperature. Therefore, the temperature could be increased by applying more voltage to the resistive heating element, simulating the heat retained by absorbing light. Afterwards, the array was to have its reflectance measured as a function of both wavelength and temperature, using equipment available at the university. Again, the temperature would be controlled using the resistive heating element. This would provide evidence for or against the memristive effect. An array without any polymer solution would go through the characterization process as well, as a control group to verify that the polymer solution is the cause of any change in radiation properties. Finally, different concentrations of the polymer solution would be tested, to determine if the memristive behavior is dependent on polymer concentration - for instance, higher concentrations may block more light than others.

Chapter 4: Results

Discussed in this section will be the preliminary results from our initial simulations. Explained will be the variables tested in our simulations, and the changes watched for by our team in the resulting analysis.

4.1 Simulations

In order to expand the silver nanorod arrays physically, and measure the resulting change in transmission, we decided on a method where the arrays which we would print would subsequently be immersed in a polymer solution which would expand given an introduction of heat. This expansion within the solution would cause for the negative space between the silver nanorods in the array to lengthen, which, given our initial claim, would result in a change in transmissivity of light through the array. The following simulations were run in order to see if the desired results would be acquired, before any geometries were fabricated.

In the actual simulations, energy was measured by monitors placed in the simulation space. Every monitor has a normal vector, which is assumed to the the direction light will travel. Out simulations did not consistently have light passing in this manner. If light is moving antiparallel to the monitor vector, they monitor

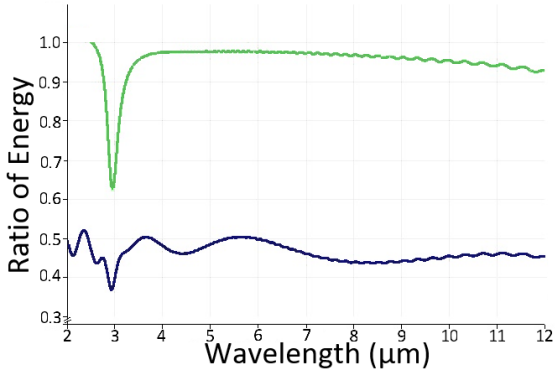

Figure 4.1: Radiation properties of array immersed in water.

records a negative value. All negative values have been removed below, in the raw data sets.

4.1.1 Immersion Simulation

The above graph, Figure 4.1, depicts transmission (green) and reflection (blue) in incident light frequency by microns of an array. In the above simulation, the conditions set were for the array a single nanorod with Bloch boundary conditions, with a pitch of 2.8 microns , a height of 1.2 microns, and a substrate thickness of 0.05 microns. The substrate is the metallic base printed which the silver nanorods are subsequently printed upon. We simulated the substrate as being comprised of silver as well. In the above simulation, the negative space between the rods was set to contain water. The spike downwards on the graph depicts a sudden, narrow, sizable decrease in transmission for a specific frequency of light.

Figure 4.1 shows that the extreme decrease in transmissivity at specific wavelengths of light is still expressed while the array is immersed in water. From this graph the team was able to determine that a polymer solution could be introduced

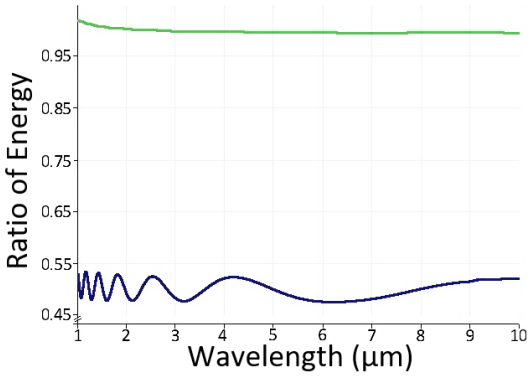

Figure 4.2: Photoeletric response of array with substrate thickness .05 μm. Little variance in either type of response.

onto the array in order to achieve our expansion, provided that the dissolution of the chosen polymer does not drastically change the radiation properties of the water. In the immersion above it can also be interpreted that since the reflection does not spike upward at the same wavelength that transmission spikes downward, the wavelengths of the reflection are absorbed more readily by the array.

4.1.2 Substrate Thickness Simulations

Substrate thickness was another parameter of the geometry that was explored in simulation. The array must be printed on a surface; however, the thickness of the substrate could influence the radiation properties, especially if it is a conductor. Silver, the planned substrate, is a conductor, so this factor had to be quantified. The substrate had to be thick enough to withstand the physical stress of expansion when immersed in a polymer solution with which heat was applied. However, the team used simulations to figure out whether differing thickness in the substrate would materially effect either transmissivity or reflectivity. The graph above, Figure 4.2,

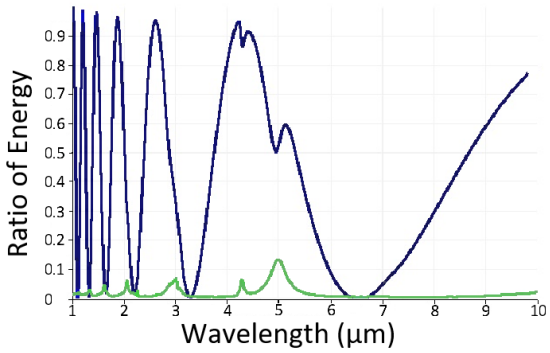

Figure 4.3: Radiation properties of array with substrate thickness 1 μm. Much greater variance based on light wavelength.

depicts the transmission (green) and reflection (blue) in incident light wavelength in microns. In Figure 4.2, the silver nanorod array has a substrate thickness 0.05 μm, 3.4 μm of height, and 2.6 μm pitch. This particular geometry was subsequently rejected, as it was simulated severely reduce the amplitude of oscillation in transmission or reflection, as seen in Figure 4.2. Similar simulations in changing the substrate thickness within 0.05 to 0.1 returned the same results: little to no variance of radiation properties.

Figure 4.3 shows a simulation with identical setup to Figure 4.2. The geometry again has a height of 3.4 microns, and pitch of 2.6 microns. However, the substrate was changed to be 1 micron thick, 20 times thicker than in Figure 4.2 (0.05 microns previously). Figure 4.3 expresses the same spike in reflection and transmission at 5 microns that the immersion simulation exhibited. Because of the great variance in the radiation properties to different light frequencies, we elected to use this substrate thickness (1 micron) in the rest of our simulations. Figure 4.3 shows offsets diverse from Figure 4.2, due to the monitors used facilitated in opposite directions. Also expressed is an almost complete absorption of light at micron 6.7, which is a bandgap

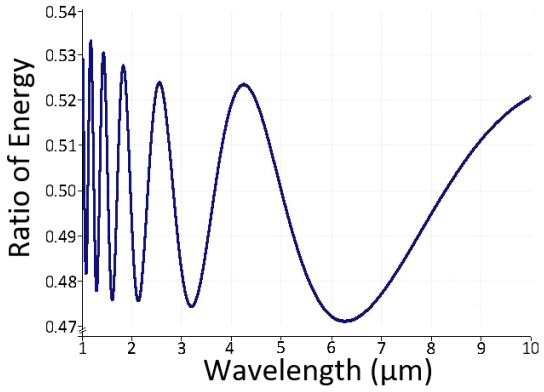

Figure 4.4: Reflectance of array with pitch 3.2 μm. The shape is similar to the prior figure.

of the material simulated. At this wavelength, all light was absorbed by the metal instead of being allowed to interact with the array.

4.1.3 Pitch Based Reflectivity Simulation

This simulation is a reflectivity graph of our silver nanorod model. This geometry had the following specifications: a height of 3.4 microns, a pitch of 3.2 microns, and a substrate thickness of 1 micron, identical to the thickness simulated in Figure 4.3. In this simulation the effect of pitch was being tested on reflection, the peak spike in reflection between microns 4 and 5 is at a wavelength 0.1 microns less that the 2.6 pitch result in Figure 4.3. This expression proves a relationship between the pitch of the silver nanorod model as its effect on radiation properties in the energy flows. If one were to take Figure 4.4 and superimpose the image on Figure 4.3 with the x axis aligned, the two shapes would mostly line up. However, the shape Figure 4.4 will be slightly compressed compared to that Figure 4.3. This demonstrates the principle by which our arrays operate.

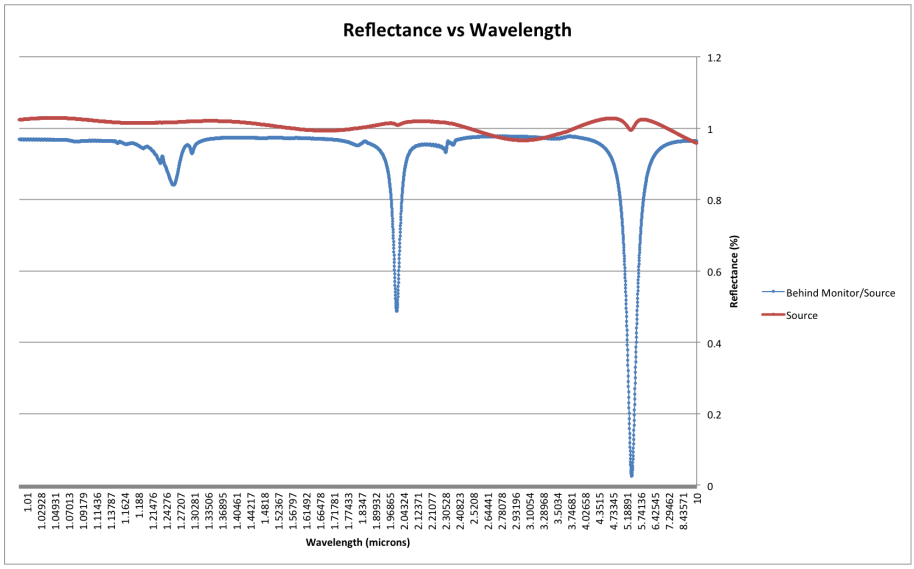

Figure 4.5: Absolute reflectance as a function of wavelength. The downward spikes are regular on an approximately exponential x axis.

4.1.4 Reflectance of Array by Frequency

Based on the raw data collected throughout our simulations (Figures 5.6, 5.7, and 5.8) we were able to condense the information into a graph of the actual reflectance of the array, based on the frequency. Figure 4.5 depicts the source energy for the wavelength (red), in relation to the reflected energy (blue). The graph is a conversion of the rather abstract data extracted by the monitors into more easily understood numbers; the reflectance is now a simple ratio of source energy and reflected energy. The source should be exactly at one. However, the reconstruction did not account for any possible absorption of light, meaning that it did not always add to the same value. This accounts for the apparent nonphysical source.

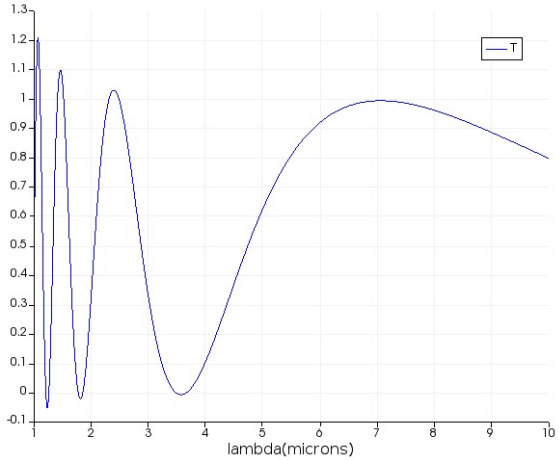

Figure 4.6: Plot of energy flow through a monitor placed directly in front of the source. Includes both pre-incident and reflected light.

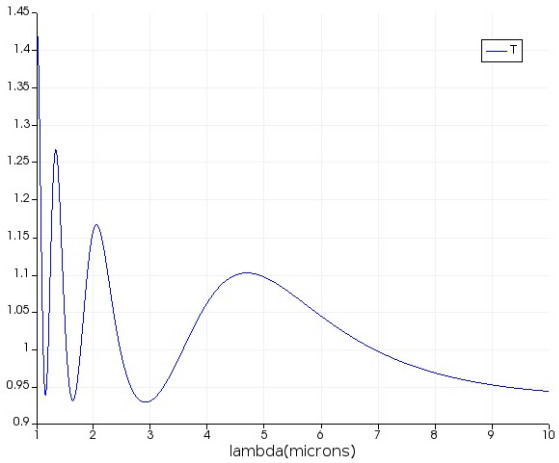

Figure 4.7: Plot of energy flow through a monitor placed directly behind the source. Includes only reflected light.

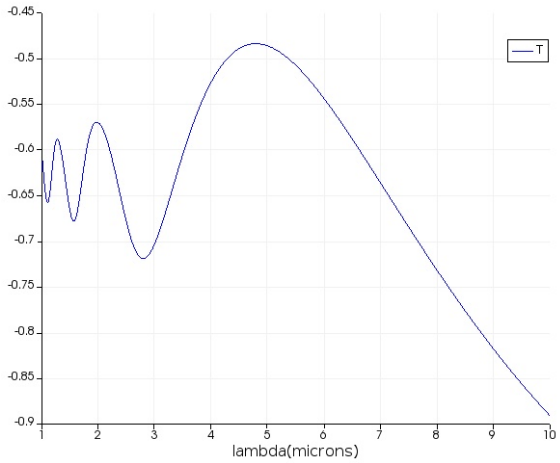

Figure 4.8: Plot of calculated absolute reflectance, created by subtracting the data from the monitor behind the source from the data from the monitor in front of the source.

4.2 Experiment

Due to repeated delays in procuring the arrays initially, among other logistical issues, the team did not quite reach the measurement stage detailed in Section 4.2.3. As of this writing, the desired effect has not been seen under the microscope. As mentioned above, this was a desirable prerequisite to characterizing the array. For that reason, there is no data that can be provided to either confirm or refute our idea. Nonetheless, the equipment is in position to both see the effect visually, and measure it quantitatively. Unfortunately, there is little room for discussion, due to the lack of data at this point. Nonetheless, this report details enough progress for any team in the future to move forward with.

Chapter 5: Conclusion

As demonstrated above, the team has extensively simulated the properties of silver nanorod arrays. These results agree with those measured by Malerba et. al.,[9] at least as far as the simulations are approximately the same. They clearly indicate that a variable pitch can be exploited to create a memristive effect. The team proposed to approximate a variable pitch by enveloping the array in a thermally expansive polymer, such that the tops of the rods bent out at angles. The arrays were constructed and enveloped in a solution, but no definitive data was collected to indicate either success or failure, due to logistical issues. Further work should immediately build off of this, and either confirm or deny the effect. As discussed in the measurement section, Section 4.2.3, there is a great deal of work that can be done to explore this effect further, should it indeed exist. Work should then be done to move away from an external heating source, and miniaturize the array, so as to provide a memristor for a photonic circuit that is usable in the visible regime.

Bibliography

[1] Gins Lifante. *Integrated Photonics Fundamentals*. English. Wiley. ISBN: 0-470-84868-5. URL: http://opt.zju.edu.cn/zjuopt21/attachments/rar/cksj/qt/1%20(7).pdf (visited on 03/03/2017).

[2] Tom Simonite. *Computing at the Speed of Light*. URL: https://www.technologyreview.com/s/420082/computing-at-the-speed-of-light/ (visited on 03/03/2017).

[3] L. Chua. "Memristor-The missing circuit element". In: *IEEE Transactions on Circuit Theory* 18.5 (Sept. 1971), pp. 507–519. ISSN: 0018-9324. DOI: 10.1109/TCT.1971.1083337.

[4] D. Li et al. "Identifying Opportunities for Byte-Addressable Non-Volatile Memory in Extreme-Scale Scientific Applications". In: *2012 IEEE 26th International Parallel and Distributed Processing Symposium*. May 2012, pp. 945–956. DOI: 10.1109/IPDPS.2012.89.

[5] Hongya Wu et al. "Microwave Memristive-like Nonlinearity in a Dielectric Metamaterial". In: *Scientific Reports* 4 (June 2014). ISSN: 2045-2322. DOI: 10.1038/srep05499. URL: http://www.nature.com/articles/srep05499 (visited on 10/18/2016).

[6] C. Hoessbacher et al. "The plasmonic memristor: a latching optical switch". In: *Optica* 1.4 (Oct. 20, 2014), pp. 198–202. ISSN: 2334-2536. DOI: 10.1364/OPTICA.1.000198. URL: https://www.osapublishing.org/abstract.cfm?uri=optica-1-4-198 (visited on 03/03/2017).

[7] J. D. Baena. "Resonating elements longer than the unit cell: A way to make very dense broadband left-handed metamaterials". In: *2015 9th International Congress on Advanced Electromagnetic Materials in Microwaves and Optics (METAMATERIALS)*. Sept. 2015, pp. 361–363. DOI: 10.1109/MetaMaterials.2015.7342451.

[8] Tie Cui, David Smith, and Ruopeng Liu. *Metamaterials Theory, Design and Application*. Springer, 2010. ISBN: 978-1-4419-0572-7.

[9] Mario Malerba et al. "3D vertical nanostructures for enhanced infrared plasmonics". In: *Scientific Reports* 5 (Nov. 10, 2015), p. 16436. DOI: 10.1038/srep16436. URL: https://www.nature.com/articles/srep16436 (visited on 03/29/2019).

[10] P. Prucnal, M. Santoro, and Ting Fan. "Spread spectrum fiber-optic local area network using optical processing". In: *Journal of Lightwave Technology* 4.5 (May 1986), pp. 547–554. ISSN: 0733-8724. DOI: 10.1109/JLT.1986.1074754.

[11] Vanya Arun et al. "Design and performance analysis of multiple all optical logic gates in a single photonic circuit". en. In: *Optical and Quantum Electronics* 48.1 (Jan. 2016), p. 36. ISSN: 0306-8919, 1572-817X. DOI: 10.1007/s11082-015-0334-8. URL: https://link.springer.com/article/10.1007/s11082-015-0334-8 (visited on 03/03/2017).

[12] Mohammad Rakib Uddin et al. "Micro-photonic NOT and NOR Gates". In: *Advanced Photonics 2016 (IPR, NOMA, Sensors, Networks, SPPCom, SOF) (2016), paper JTu4A.4*. Photonic Networks and Devices. Optical Society of America, July 18, 2016, JTu4A.4. DOI: 10.1364/IPRSN.2016.JTu4A.4. URL: https://www.osapublishing.org/abstract.cfm?uri=Networks-2016-JTu4A.4 (visited on 03/28/2019).

[13] Dmitri B. Strukov et al. "The missing memristor found". In: *Nature* 453.7191 (May 1, 2008), pp. 80–83. ISSN: 0028-0836. DOI: 10.1038/nature06932. URL: http://www.nature.com/nature/journal/v453/n7191/full/nature06932.html?cookies=accepted (visited on 10/18/2016).

[14] Rostislav V. Lapshin. "An improved parametric model for hysteresis loop approximation". In: *arXiv:1701.08070 [physics]* (Jan. 27, 2017). arXiv: 1701.08070. URL: http://arxiv.org/abs/1701.08070 (visited on 03/28/2019).

[15] P. Mazumder, S. M. Kang, and R. Waser. "Memristors: Devices, Models, and Applications [Scanning the Issue]". In: *Proceedings of the IEEE* 100.6 (June 2012), pp. 1911–1919. ISSN: 0018-9219. DOI: 10.1109/JPROC.2012.2190812.

[16] Y. Ho, G. M. Huang, and P. Li. "Dynamical Properties and Design Analysis for Nonvolatile Memristor Memories". In: *IEEE Transactions on Circuits and Systems I: Regular Papers* 58.4 (Apr. 2011), pp. 724–736. ISSN: 1549-8328. DOI: 10.1109/TCSI.2010.2078710.

[17] S. Mittal, J. S. Vetter, and D. Li. "A Survey Of Architectural Approaches for Managing Embedded DRAM and Non-Volatile On-Chip Caches". In: *IEEE Transactions on Parallel and Distributed Systems* 26.6 (June 2015), pp. 1524–1537. ISSN: 1045-9219. DOI: 10.1109/TPDS.2014.2324563.

[18] Roberto Marani, Gennaro Gelao, and Anna Gina Perri. "A review on memristor applications". In: *arXiv:1506.06899 [cond-mat]* (June 23, 2015). arXiv: 1506.06899. URL: http://arxiv.org/abs/1506.06899 (visited on 03/28/2019).

[19] S. Shin, K. Kim, and S. M. Kang. "Memristor Applications for Programmable Analog ICs". In: *IEEE Transactions on Nanotechnology* 10.2 (Mar. 2011), pp. 266–274. ISSN: 1536-125X. DOI: 10.1109/TNANO.2009.2038610.

[20] J. B. Pendry. "Negative Refraction Makes a Perfect Lens". In: *Physical Review Letters* 85.18 (Oct. 2000), pp. 3966–3969. DOI: 10.1103/PhysRevLett.85.3966. URL: http://link.aps.org/doi/10.1103/PhysRevLett.85.3966 (visited on 09/23/2016).

[21] D. R. Smith et al. “Composite Medium with Simultaneously Negative Permeability and Permittivity”. In: *Physical Review Letters* 84.18 (May 2000), pp. 4184–4187. DOI: 10.1103/PhysRevLett.84.4184. URL: http://link.aps.org/doi/10.1103/PhysRevLett.84.4184 (visited on 09/19/2016).

[22] Stefan Enoch et al. “A Metamaterial for Directive Emission”. In: *Physical Review Letters* 89.21 (Nov. 2002), p. 213902. DOI: 10.1103/PhysRevLett.89.213902. URL: http://link.aps.org/doi/10.1103/PhysRevLett.89.213902 (visited on 09/19/2016).

[23] Yanhong Zou et al. “Enhancing and tuning absorption properties of microwave absorbing materials using metamaterials”. In: *Applied Physics Letters* 93.26 (Dec. 29, 2008), p. 261115. ISSN: 0003-6951. DOI: 10.1063/1.3062854. URL: https://aip.scitation.org/doi/10.1063/1.3062854 (visited on 03/28/2019).

[24] Terence Shepherd and Paul Tapster. “Dielectric media”. Pat. US20030151033 A1. U.S. Classification 252/570; International Classification G02B6/12, B29C69/02, B29C67/00, G02B6/122, B29C39/10; Cooperative Classification B29K2995/0073, B29K2995/0094, B29C69/02, G02B6/1225, B29C67/0092, G02B6/1221, B82Y20/00, B29C67/0081, B29C39/10, G02B2006/1219, B29C2791/001, B29K2995/0006; European Classification B82Y20/00, B29C67/00R6, G02B6/122P, G02B6/122C, B29C39/10, B29C69/02, B29C67/00R8D. Aug. 2003. URL: http://www.google.com/patents/US20030151033 (visited on 09/23/2016).

[25] Dexin Ye et al. “Microwave gain medium with negative refractive index”. In: *Nature Communications* 5 (Dec. 2014), p. 5841. ISSN: 2041-1723. DOI: 10.1038/ncomms6841. URL: http://www.nature.com/doifinder/10.1038/ncomms6841 (visited on 09/19/2016).

[26] Md Moinul Islam et al. “A Miniaturized Antenna with Negative Index Metamaterial Based on Modified SRR and CLS Unit Cell for UWB Microwave Imaging Applications”. en. In: *Materials* 8.2 (Jan. 2015), pp. 392–407. DOI: 10.3390/ma8020392. URL: http://www.mdpi.com/1996-1944/8/2/392 (visited on 09/19/2016).

[27] M. R. Soheilifar. “Design, fabrication, and characterization of scaled and stacked layers metamaterial absorber in microwave region”. en. In: *Microwave and Optical Technology Letters* 58.5 (May 2016), pp. 1187–1193. ISSN: 1098-2760. DOI: 10.1002/mop.29762. URL: http://onlinelibrary.wiley.com/doi/10.1002/mop.29762/abstract (visited on 09/25/2016).

[28] Collin Ladd et al. “3D Printing of Free Standing Liquid Metal Microstructures”. en. In: *Advanced Materials* 25.36 (Sept. 2013), pp. 5081–5085. ISSN: 1521-4095. DOI: 10.1002/adma.201301400. URL: http://onlinelibrary.wiley.com/doi/10.1002/adma.201301400/abstract (visited on 09/27/2016).

[29] Xu Zhang et al. "Broadband plasmonic metamaterial absorber with fish-scale structure at visible frequencies". en. In: *Optical Materials Express* 6.7 (July 2016), p. 2448. ISSN: 2159-3930. DOI: 10.1364/OME.6.002448. URL: https://www.osapublishing.org/abstract.cfm?URI=ome-6-7-2448 (visited on 09/27/2016).

[30] Abhijit Biswas et al. "Advances in topdown and bottomup surface nanofabrication: Techniques, applications & future prospects". In: *Advances in Colloid and Interface Science* 170.12 (Jan. 2012), pp. 2–27. ISSN: 0001-8686. DOI: 10.1016/j.cis.2011.11.001. URL: http://www.sciencedirect.com/science/article/pii/S0001868611001904 (visited on 03/03/2017).

[31] Alexandre Baron et al. "[INVITED] Self-assembled optical metamaterials". In: *Optics & Laser Technology* 82 (Aug. 2016), pp. 94–100. ISSN: 0030-3992. DOI: 10.1016/j.optlastec.2016.02.024. URL: http://www.sciencedirect.com/science/article/pii/S0030399216301153 (visited on 03/03/2017).

[32] P. Rai-Choudhury. *Handbook of Microlithography, Micromachining, and Microfabrication: Microlithography*. en. IET, Jan. 1997. ISBN: 978-0-85296-906-9.

[33] Weiling Dong et al. "Wideband Absorbers in the Visible with Ultrathin Plasmonic-Phase Change Material Nanogratings". In: *The Journal of Physical Chemistry C* 120.23 (June 2016), pp. 12713–12722. ISSN: 1932-7447. DOI: 10.1021/acs.jpcc.6b01080. URL: http://dx.doi.org/10.1021/acs.jpcc.6b01080 (visited on 09/27/2016).

[34] Robert Nidetz. "The Self-Assembly of Nanogold for Optical Metamaterials." In: (2011).

[35] Evgeniy Shkondin et al. "Fabrication of high aspect ratio TiO2 and Al2O3 nanogratings by atomic layer deposition". In: *Journal of Vacuum Science & Technology A* 34.3 (May 2016), p. 031605. ISSN: 0734-2101, 1520-8559. DOI: 10.1116/1.4947586. URL: http://scitation.aip.org/content/avs/journal/jvsta/34/3/10.1116/1.4947586 (visited on 09/27/2016).

[36] Arijit Gandhi et al. "Studies on thermoresponsive polymers: Phase behaviour, drug delivery and biomedical applications". In: *Asian Journal of Pharmaceutical Sciences* 10.2 (Apr. 2015), pp. 99–107. ISSN: 1818-0876. DOI: 10.1016/j.ajps.2014.08.010. URL: http://www.sciencedirect.com/science/article/pii/S1818087614000634.

[37] Jianfeng Zhou et al. "Correlation between Dielectric/Electric Properties and Cross-Linking/Charge Density Distributions of Thermally Sensitive Spherical PNIPAM Microgels". In: *Macromolecules* 45.15 (Aug. 2012), pp. 6158–6167. ISSN: 0024-9297. DOI: 10.1021/ma300454h. URL: https://doi.org/10.1021/ma300454h (visited on 03/06/2019).

[38] Mitsuhiro Shibayama, Tomohisa Norisuye, and Shunji Nomura. "Cross-link Density Dependence of Spatial Inhomogeneities and Dynamic Fluctuations of Poly(N-isopropylacrylamide) Gels". In: *Macromolecules* 29.27 (Jan. 1996), pp. 8746–8750. ISSN: 0024-9297. DOI: 10.1021/ma9609994. URL: https://doi.org/10.1021/ma9609994 (visited on 03/06/2019).

[39] Mitsuhiro Shibayama, Yoshihiro Fujikawa, and Shunji Nomura. "Dynamic Light Scattering Study of Poly(N-isopropylacrylamide-co-acrylic acid) Gels". In: *Macromolecules* 29.20 (Jan. 1996), pp. 6535–6540. ISSN: 0024-9297. DOI: 10.1021/ma960320w. URL: https://doi.org/10.1021/ma960320w (visited on 03/06/2019).

[40] *Nanophotonic FDTD Simulation Software - Lumerical FDTD Solutions*. URL: https://www.lumerical.com/products/fdtd-solutions/ (visited on 03/30/2019).

[41] *Nanoscribe Photonic Professional GT | Terrapin Works*. URL: https://terrapinworks.umd.edu/equipment/nanoscribe-photonic-professional-gt (visited on 03/30/2019).

[42] *MilliporeSigma | United States | Sigma-Aldrich*. URL: https://www.sigmaaldrich.com/united-states.html (visited on 03/31/2019).